INSTITUTE OF PHYSICS PUBLISHING JOURNAL OF PHYSICS: CONDENSED MATTER

J. Phys.: Condens. Matter **18** (2006) 6085–6093 doi:10.1088/0953-8984/18/26/026

Magnetotransport properties depending on the nanostructure of Fe_3O_4 nanowires

M Abid[1], **J-P Abid, S Jannin, S Serrano-Guisan, I Palaci and J-Ph Ansermet**

IPN/SB, Ecole Polytechnique Fédérale de Lausanne, station 3, CH-1015, Lausanne, Switzerland

E-mail: mabid@chimie.u-strasbg.fr

Received 19 March 2006, in final form 23 May 2006
Published 19 June 2006
Online at stacks.iop.org/JPhysCM/18/6085

Abstract

We have studied the magnetic behaviour of Fe_3O_4 nanowires (NWs) with two different diameter ranges, above 150 nm and below 60 nm, made by electrodeposition techniques into a polymeric template. The nanowires were characterized using various techniques, in particular Mössbauer and thermoelectrical power measurements. The stoichiometric distribution of Fe cations showed clearly the presence of the magnetite inverse spinel electronic structure. Structural analysis performed using high-resolution transmission electron microscopy revealed two kinds of nanowire morphologies depending on the size. For nanowires above 150 nm in diameter, a contiguous network of well-bound nanoparticles was obtained. Instead, with a diameter of 60 nm, a polycrystalline structure was observed. The largest nanowires presented a magnetoresistance (MR) greater than 10%, whereas the thinner nanowires had almost none.

1. Introduction

In the last decade considerable interest has developed in all effects related to spin-dependent transport like giant magnetoresistance (GMR) [1, 2] and tunnelling magnetoresistance (TMR) [3]. Hence, the half-metallic character of ferromagnetic oxide, in particular magnetite [4], nanomaterials appears to be quite promising for applications in spintronics. This theoretically perfect spin-polarization, together with its relatively high Curie temperature, might be exploited in a variety of advanced devices such as highly sensitive magnetic sensors (e.g. read heads for magnetic recording). Magnetite should considerably enhance the efficiency of these devices, in which the current spin-polarizing materials can only achieve about 40%. Non-perfect magnetite crystals have the particularity of being composed of small islands of stoechiometrically perfect crystallinity separated by anti-phase boundaries (APB) [5, 6].

[1] Author to whom any correspondence should be addressed.

These APBs result from shifts or rotations of the iron sub-lattices relative to the crystal lattice, and the magnetite islands couple either ferromagnetically or anti-ferromagnetically. This can be observed experimentally as a magnetoresistive GMR-like response [5], in a similar way to the magnetoresistance of multilayers made of magnetic and non-magnetic materials. Transfer of spin-polarised electrons between grain boundaries also gives rise to magnetoresistive effects and this has been observed in compacted magnetite powders [7]. Magnetite is also characterized by metal to insulator transition (more precisely, semiconductor–insulator or semiconductor–semiconductor) around $T_v = 110$ K, known as the Verwey transition, which is an ordering effect of the iron ions Fe^{2+} and Fe^{3+} within the B sites (octahedron sites) of the inverse spinel lattice structure. For TMR devices, the preparation of magnetite nanomaterials requires low deposition and thin film techniques. Nevertheless, the possible applications of magnetite in devices rely on the assumption that the physical properties are the same as those of bulk material. Unfortunately, the physical properties such as resistivity, magnetoresistance [8, 9] or magnetic behaviour of Fe_3O_4 strongly deviate from bulk properties. This has often been ascribed to the presence of anti-phase boundaries. In this framework, we have fabricated nanowires of different diameters and morphologies by electrodeposition using polymeric templates. The obtained results provide a clear picture of the dependence of the transport on the nanowires diameter size, shedding light on some aspects of magnetotransport depending of nanostructure morphology.

2. Experimental section

The Fe_3O_4 synthesis was achieved by means of an electroprecipitation method [10]. Typically, the electrodeposition experiment was carried out in a classical three electrode glass cell. The circuit loop was closed using a saturated Ag/AgCl electrode as a reference and a platinum wire as a counter electrode. The potential window was estimated using cyclic voltammetry. All experiments were performed at 343 K under N_2 bubbling during at least 1 h and employing the EGG 273A potentiostatic system. The morphological analysis was achieved using a Philips CM300 high-resolution transmission microscope (HRTEM) and a Philips XL30 FEG scanning electron microscope. The structural analysis of the magnetite nanomaterials was performed using a Siemens D5000 Bragg–Brentano diffractometer operating in the θ–2θ Bragg configuration. The voltage was set at 50 kV with a 45 mA flux. The electrical transport and magnetization properties were performed using nanowires typically 6 μm long with a diameter of 60 nm or above 150 nm. During the electrodeposition procedure, a single contact was made between two gold layers sputtered on both sides of the membranes. The resistance of the contacted nanowire was measured in a magnetic field of -8 kOe $< H <$ 8 kOe and in the temperature range of 70–300 K. High-precision thermoelectric power measurements by lock-in amplifier detection were carried out using a laser beam as an oscillatory source [11].

3. Results and discussion

3.1. Structural properties

Figure 1(a) shows a scanning electron micrograph of the Fe_3O_4 nanowires after removing the polycarbonate. The nanowires are about 150 nm in size with a density of 10^9 cm^{-2}. As portrayed in figure 1(b), energy-dispersive x-ray analysis confirms the magnetite stoichiometry (Fe_3O_4) with an average atomic ratio of O/Fe 1.33. The bright-field transmission micrographs display Fe_3O_4 nanowires with a diameter above 150 nm (figure 1(c)) and of 60 nm (figure 1(d)). The TEM analysis reveals that the as-prepared nanowires above 150 nm are made with

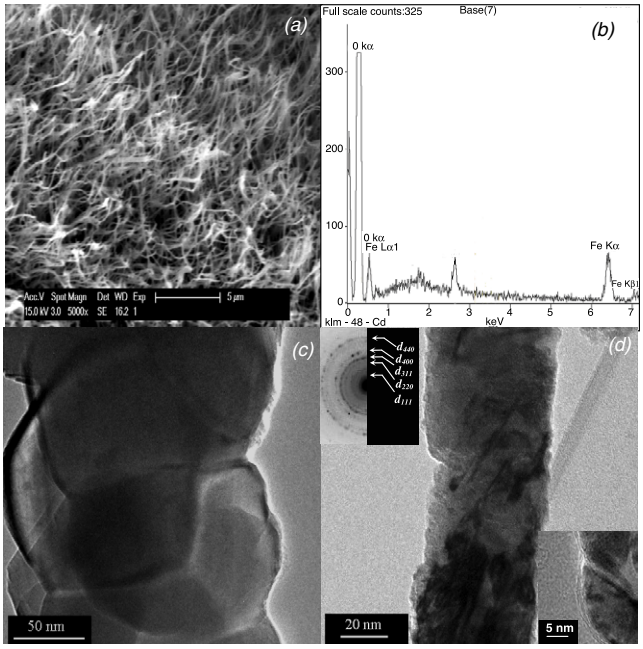

Figure 1. (a) SEM picture after removing the polycarbonate membrane, (b) EDS spectra, (c) TEM micrographs of NWs above 150 nm and (d) around 60 nm (inset shows: (left) the SAED (selected area diffraction); (right) the HRTEM micrograph).

agglomerates of nanoparticles. As shown in figure 1(c), the large nanoparticles merge together in order to form welded-neck junctions and grain boundaries. For nanowires of smaller sizes (around 60 nm), we observe granular wires containing a broad range of nanoparticle sizes (size below 10 nm). However, it must be pointed out that nanoparticles do not show the typical junction or grain boundaries between the nanoparticles (inset figure 1(d)). The magnetite structural study using SAED indicates the presence of a cubic structure of Fe_3O_4 and/or γ-Fe_2O_3 (see inset of figure 1(d)), which is consistent with the x-ray diffraction (XRD) result (not shown). XRD cannot be more specific because γ-Fe_2O_3 (maghamite) and Fe_3O_4 have similar cubic inverse spinel structure with nearly the same lattice parameter ($a = 0.8350$ and $a = 0.8396$ nm, respectively). To ensure the absence of impurities in the magnetite sample at room temperature, Mössbauer measurements on Fe_3O_4 NWs are performed and a typical result is portrayed in figure 2(a). The determination of stoichiometry using Mössbauer spectroscopy is based on the rapid electron hopping process at room temperature. Since this hopping process is much faster than the lifetime of the excited ^{57}Fe nucleus, the B site ions appear as one average '$Fe^{2.5+}$'-like component [12]. Therefore, at room temperature, the Mössbauer spectrum of Fe_3O_4 will contain only two components: one originating from the A sites containing Fe^{3+} ions, and the other from the B sites containing $Fe^{2.5+}$ ions. Each component is split into a sextet, due to hyperfine interactions between the nuclear magnetic dipole moment and the internal magnetic field caused by the ferrimagnetically ordered electron spins. A typical spectrum of Fe_3O_4 nanowires (figure 2(a)) is fitted with two sextet components yielding an IS value (relative to -Fe) of 0.2969 mm s^{-1} and B $=$ 49.53(9) for the first sextet, and IS $=$ 0.6386(6) and B $=$ 46.21(6) for the second sextet. Our fitting parameters are in good agreement with literature reports for Fe_3O_4 [13, 14]. The components with the larger B and smaller IS corresponds to the Fe^{3+} component. The intensity ratio defined by $\beta = I(3+)/I(2.5+)$ of the two components

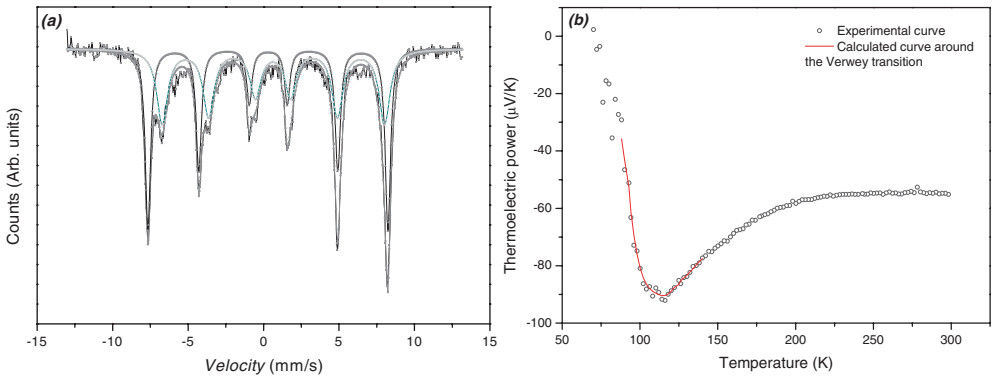

Figure 2. (a) A typical room-temperature ^{57}Fe Mössbauer spectrum of Fe_3O_4 spinel ferrite at zero field of Fe_3O_4 NWs. (b) Typical room-temperature experimental data of thermoelectrical power measurement of magnetite NWs, the calculated curves (in red) values according to the expression (2) using $2\Delta = 0.106$ eV and q_p–$q_n = 0.01$ eV.

(This figure is in colour only in the electronic version)

is a very sensitive measure of the stoichiometry [15]. This is equal to $1/2$ for stoichiometric Fe_3O_4, and goes to infinity for γ-Fe_2O_3. The non-stoichiometric value β can be related to expression (1).

Effectively, by considering the charge neutrality, we can write non-stoichiometric $Fe_{3-\alpha}O_4$ as $Fe_A^{3+}[Fe_{1+2\delta}^{3+}Fe_{1-3\delta}^{2+}\square_\delta]_B O_4^{2-}$, where $\square$ stands for a vacancy. This leads to $Fe_A^{3+}[Fe_{1-3\delta}^{3+}Fe_{1-3\delta}^{2+}Fe_{5\delta}^{3+}\square]_B O_4^{2-}$, since every vacancy traps five Fe^{3+} ions. Including hopping, we finally obtain $Fe_A^{3+}[Fe_{2-6\delta}^{2.5+}Fe_{5\delta}^{3+}\square_\delta]_B O_4^{2-}$. So, β is given by the relation:

$$\beta = \frac{1+5\delta}{2-6\delta}. \tag{1}$$

We observe a slight non-stoichiometric phase which corresponds to a composition phase $Fe_{2.96}O_4$ and $Fe_{2.97}O_4$ for 60 nm and above 150 nm diameter size nanowires, respectively.

To investigate the presence of impurities and confirm the non-stoichiometric Fe_3O_4 nanowires' character, the study of the thermoelectric properties at the Verwey transition (T_v) has been envisaged. Kuipers *et al* analysed thermoelectric power measurements on pure and doped magnetite crystals, and concluded that minor changes in stoichiometry have a deep influence on whether p- or n-type conduction is observed below T_v [17]. Figure 2(b) displays the evolution of the absolute thermoelectric power with the temperature. The thermoelectric power decreases gradually from 200 K and reaches a minimum at 115 K. At lower temperatures, the thermoelectric power increases again and becomes positive, pointing to positive charged carriers. These values of Seebeck coefficient above the Verwey transition are in good agreement with the values reported in literature [18, 19]. The thermoelectrical power results are fitted using the mixed conduction model [17]. This model consists of assuming that an energy gap exists between two kinds of electron states, localized on Fe^{2+} and Fe^{3+} ions, respectively. Thus one can distinguish two kinds of charge carriers resulting in a mixed conduction: holes in the Fe^{3+} levels and electrons on the Fe^{2+} levels. Accordingly to this model, the Seebeck coefficient can be expressed as a function of the temperature:

$$S = \frac{1}{eT}\frac{-n(\Delta-\epsilon) + P(\Delta-\epsilon)\times\mu_p/\mu_n}{n + p\times\mu_p/\mu_n} \tag{2}$$

where μ_p and μ_n are the mobilities of the p- and n-type charge carriers, respectively, which are assumed to be thermally activated, Δ represents the energy gap to create a charge carrier, and

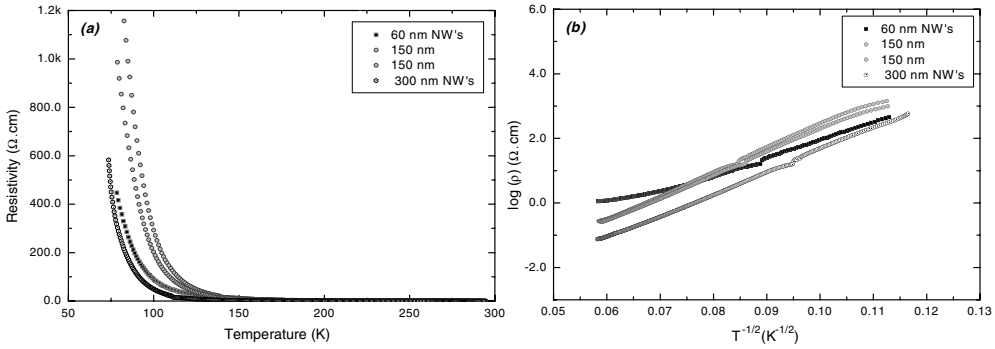

Figure 3. (a) Resistivity versus temperature with different size diameters of Fe_3O_4 NWs; (b) shows the resistivity plotted as $\log(\rho)$ versus $T^{-1/2}$.

finally γ is the cation vacancy concentration defined by $Fe^{3+}_{2+2\delta}Fe^{2+}_{1-3\delta}V_\gamma O_4$. The best fitting is obtained for q_p–$q_n = 0.01$ eV, $2\Delta = 0.09$–0.10 eV, and values of $\gamma = 0.035$ and 0.02, which correspond to the stoichiometry of $Fe_{2.96}O_4$ for 60 nm and $Fe_{2.98}O_4$ for nanowires above 150 nm, respectively. In summary, Mössbauer and thermoelectric measurements show that the Fe_3O_4 nanowires made by electrochemical methods exhibit a slight non-stoichiometric phase. We presume that this is due to the wet condition used during fabrication.

3.2. Transport properties

The temperature-dependent resistivity results are shown in figures 3(a) and (b). The electrical transport properties have been investigated for nanowires with different sizes. Room-temperature resistivities of the 60, 150 and 300 nm nanowires are 1.277, 0.281 and 0.077 Ω cm respectively, which are much higher than the value (0.0004 Ω cm) for 150 nm epitaxial grain boundaries [20]. Whatever the diameter size of the nanowire, the resistivity increases exponentially with decreasing temperature. These transport features on such nanostructures has the form of $\log[\rho] = T^{-1/2}$.

This behaviour is ascribed to a fluctuation-induced tunnelling conduction mechanism in disordered materials [21], in which the thermally activated voltage fluctuation barriers play a role in determining the temperature dependence of the conductivity. Further analysis (figure 3(b)) shows that decreasing the diameter of the nanowires induces an increase in the resistivity. Such behaviour can be understood by introducing the fact that, when the diameter of the nanowire is in the range of, or smaller than, the mean free path of the electrons, the electrical resistivity of the conductor will increase [22]. Similar behaviour has been reported on granular Fe_3O_4 thin film by Liu *et al* [23]. In the present case, for nanowires with a diameter of around 60 nm, the higher resistivity observed in the temperature range from 300 to 160 K can be attributed to the diffusive scattering of the conduction electrons at the surface. Finally, contrary to the 'bulk' Fe_3O_4 material, no sharp Vervey transition [24] is observed. Park *et al* [25] suggest that the tunnelling effect due to the grain boundaries can causes the disappearance of the Verwey transition.

3.3. Magnetic properties

Figures 4(a) and (b) show the magnetization loops of Fe_3O_4 nanowires for different diameters (60 nm and above 150 nm, respectively) measured at 3 and 300 K for parallel magnetic fields.

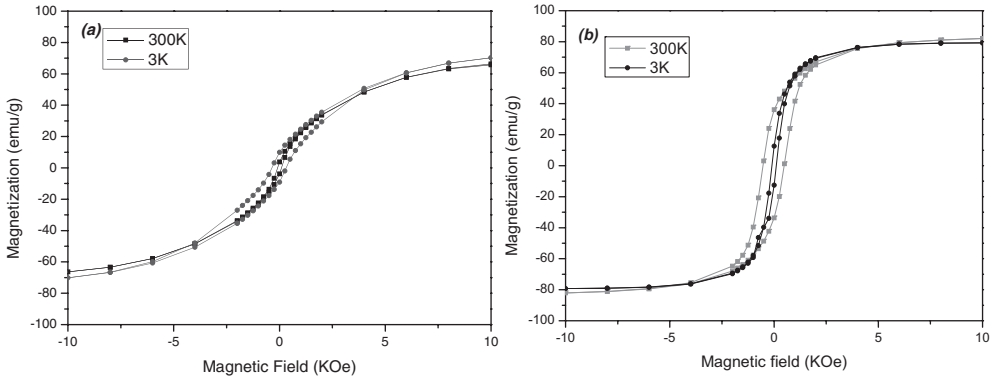

Figure 4. Hysteresis loops at 3 and 300 K for (a) 60 nm and (b) above 150 nm Fe_3O_4.

Changing the magnetic field orientation induces no modification of the magnetization. The Fe_3O_4 nanowires with a diameter above 150 nm show a different shape in the hysteresis loop compared to the 60 nm Fe_3O_4 nanowire samples. Typically, the hysteresis obtained for nanowires above 150 nm quickly reaches saturation at low field. For the 60 nm diameter nanowires, the magnetization does not saturate up to MH = 50 kOe and the value at MH = 10 kOe is about 0.85 times MH = 50 kOe (3 K). Moreover, the magnetization values are only slightly smaller than the bulk saturation magnetization at 0 K (95 emu g^{-1}) whatever the nanowire size. We can note that the coercitivity (H_c) decreases with the diameter of the nanoparticles. Magnetization measurements as a function of temperature are performed according to the zero-field-cooling (ZFC)–field-cooling (FC) procedure. M_{ZFC} was measured on warming from 3 to 300 K, whereas M_{FC} was recorded during the subsequent cooling. Figures 5(a) and (b) show the results obtained for nanowires with different sizes. For measurements at $H_{appl} < 750$ Oe, an irreversible magnetic behaviour (a difference between M_{FC} and M_{ZFC}) is observed over the whole temperature range.

Let us now consider the $[-d(M_{FC} - M_{ZFC})/dT]$ curves (figure 5(c)). It is worth recalling that, in the presence of independent relaxation phenomena (i.e. non-interacting particles), the temperature derivative of the remnant magnetization reflects the effective distribution of anisotropy energy barriers of the system [27]. A common feature of all theses curves is the presence of two peaks more or less well defined with the applied field—a small peak T_b around the Verwey transition (∼120 K) arising out of an order–disorder transformation. More specifically, below this transition temperature, the cations on the octahedral sites start getting ordered, thus bringing about a lowering of the magnetization (see figures 5(a) and (b)). A second peak at around $T_a \sim 25$ K is consistent with the hypothesized picture of a frozen, disordered magnetic state [28] which does not depend significantly on the magnetic field. This is also confirmed by the lack of magnetization relaxation below $T_a \sim 25$ K, as shown in figure 5(d). Below T_a, the Fe_3O_4 moments do not relax and are frozen in the spin-glass-like state. On increasing the temperature above T_a, such a completely frozen state evolves into a regime where the Fe_3O_4 becomes progressively unfrozen, according to the distribution of effective anisotropy energy barriers determined by the size and by the strength of the magnetic interaction with the surroundings. On this basis, we can conveniently describe our system as being constituted by two different components: a non-relaxing (quasistatic) ferromagnetic component and a relaxing spin surface corresponding to the amorphous surface surrounding the grains. In other words, it can be assumed that the shell of the nanoparticles is characterized by a random magnetic anisotropy.

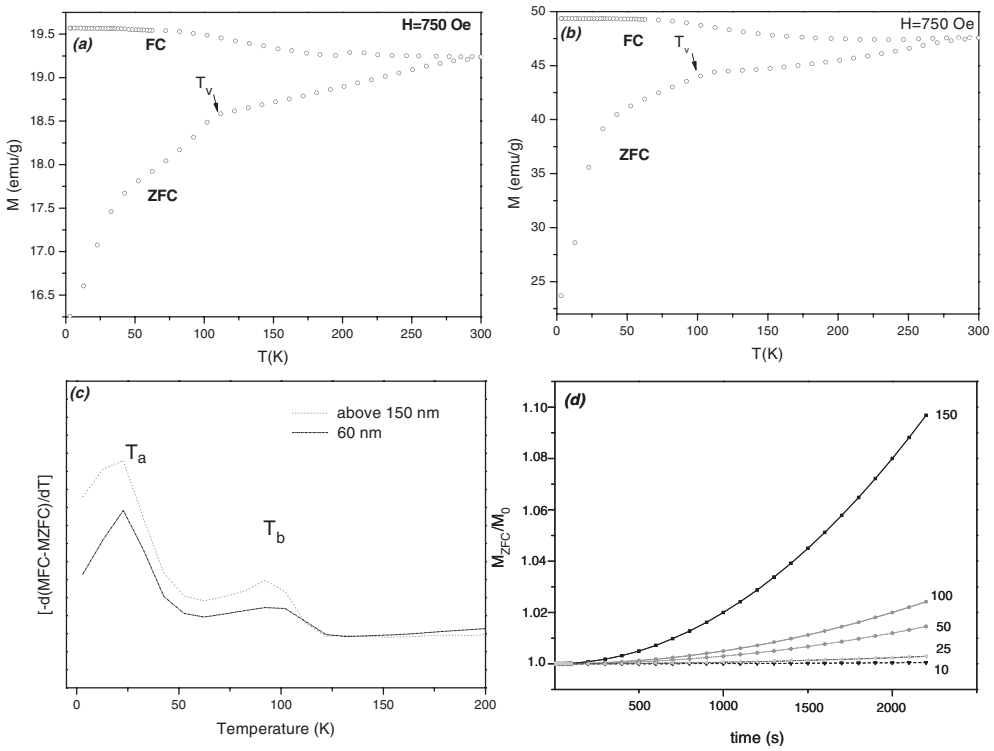

Figure 5. Zero-field-cooling (ZFC, lower branch of each curve) and field-cooling (FC, upper branch) magnetizations (M) as a function of temperature measured on (a) 60 nm and (b) above 150 nm Fe_3O_4 NWs; (c) temperature derivative $[-\mathrm{d}(M_{\mathrm{FC}} - M_{\mathrm{ZFC}})/\mathrm{d}T]$ of the difference between field-cooled and zero-field-cooled magnetizations measurements; (d) M_{ZFC} as a function of time measured on Fe_3O_4 (60 nm) NWs for $H_{\mathrm{appl}} = 100$ Oe at the indicated temperatures. M_0 is the magnetization at the beginning of the measurements.

3.4. Magnetotransport properties

Figures 6 and 7 show the longitudinal magnetoresistance ($\mathrm{MR} = (\rho_{\mathrm{h}} - \rho_0)/(\rho_0)$) of Fe_3O_4 nanowires (for diameters above 150 and 60 nm, respectively) performed at different temperatures.

The MR ratio (around 7%) observed at room temperature for nanowire diameters above 150 nm is the highest value of Fe_3O_4 reported at 8 kOe. Figure 6(b) shows the MR ratio of Fe_3O_4 nanowires measured at various temperatures. The MR ratio increases monotonically with decreasing temperature up to a maximum value at around 120 K, and then for temperatures below 90 K a clear decrease (from 12.5% at 120 K to 10.3% at 50 K) is observed. The MR curves (figure 6(a)) show exponential decreases with the magnetic field, and a saturation trend. The maximum MR occurs near the coercive field because of the randomly oriented grains. This MR behaviour obeys the relationship $\mathrm{MR} - (M/M_{\mathrm{s}})^2$ (figure 6(a)) for a non-interacting granular system. If no interaction occurred between the grains, the tunnelling conductance between adjacent grains would be proportional to $\langle \cos \phi_{i,j} \rangle$, where $\phi_{i,j}$ is the angle between the magnetization directions of grains i and j. The averaging over the grains can be expressed by $\mathrm{MR} \propto \langle \cos(\phi_{i,j}) \rangle \langle \cos(\theta) \rangle \propto -(M/M_{\mathrm{s}})^2$, where θ is the angle between the magnetization directions of the nanoparticles [29, 30].

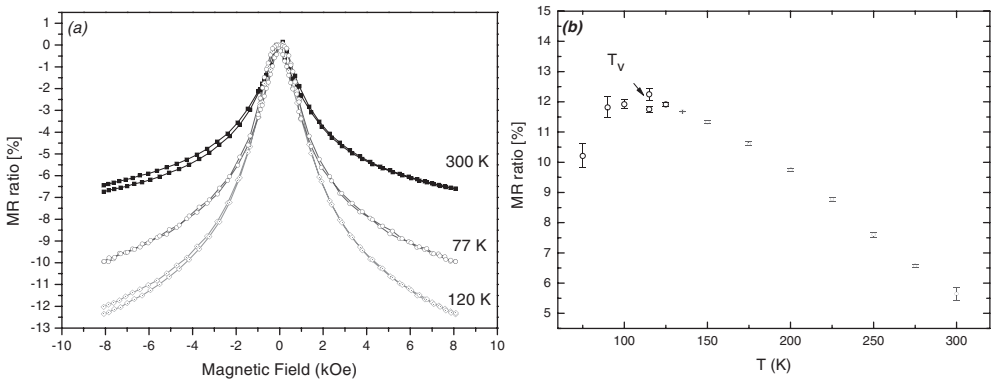

Figure 6. MR for magnetite NW's at different temperature (a) above 150 nm (b) temperature dependence of the MR at 8 kOe.

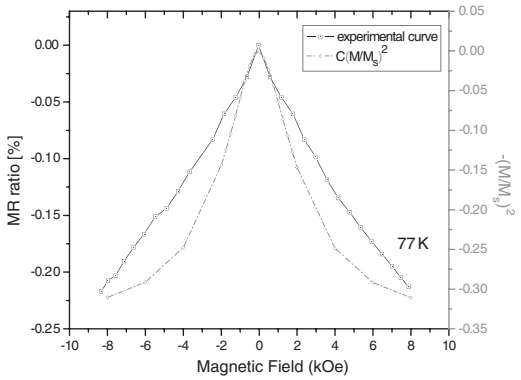

Figure 7. MR for magnetite NWs at 77 K for 60 nm and the $-(M/M_s)^2$ curve versus applied field.

In contrary, for the 60 nm diameter nanowires (figure 7), we did not observe a magnetoresistance at room temperature and only a small magnetoresistance at 77 K (around 0.2%). Here, MR curves show a quasi-linear dependence with applied magnetic field up to 8 kOe. A similar MR behaviour has been reported for Fe_3O_4 thin film (17 nm) [25] and for the core–shell Fe–Fe oxide system where the core was of Fe and the shell was of Fe oxide [31]. Moreover, as the diameter decreases, the deviation increases between the experimental MR and the calculated MR curves of the non-interacting grains. Such behaviour can be explained by the fact that large nanoparticles have a more uniform magnetization than the smaller grains. Effectively, the quality and the grain size in the Fe_3O_4 nanowires will depend strongly of the diameter of the nanotemplates. It is found that the crystallinity of small Fe_3O_4 nanowires is relatively poor, with a significant amorphous phase. In the case of small nanowires (small grains), the surface spin disorder phase in the grain boundaries will be more predominant. In summary, this study of transport properties carried out on Fe_3O_4 nanowires with different sizes and morphologies suggests that the large negative MR observed for magnetite nanowires above 150 nm in diameter can be accounted for by spin-dependent tunnelling through a network of contiguous nanoparticles. In zero magnetic fields, the magnetization (M) of each nanoparticle is oriented randomly, inducing a spin-disordered state. The application of an external magnetic field aligns all the magnetic moments and reduces the spin disorder in the case of large grains.

Consequently, there is an increase in the spin-dependent tunnelling probability, which leads to a reduction in resistance. When the particles size decreases (nanowires of 60 nm), the surface effect is more and more important and affects the magnetotransport properties.

4. Conclusion

We have studied two types of nanostructured magnetite produced by electrodeposition. Bright-field images of electron microscopy showed contiguous well-bound nanoparticles for Fe_3O_4 nanowires with diameters above 150 nm. Smaller nanowires (of around 60 nm) exhibit a polycrystalline structure. The stoichiometry of the Fe_3O_4 phase has been investigated by Mössbauer spectroscopy and thermoelectrical measurements, which definitively confirm the formation of Fe_3O_4 in a slight non-stoichiometric phase. Zero-field cooled measurements show evidence of the Verwey transition, which is also seen in the temperature dependence of the MR. The largest nanowires have the characteristics of a granular system: small saturation field and large magnetoresistance. The smallest nanowires do not saturate at 8 kOe, and have a small magnetoresistance which does not correlate to the magnetization, as in a granular system. Effectively, in this case we expect that the magnetoresistance is affected by the surface spin disorder.

References

[1] Baibich M N, Broto J M, Fert A, Nguyen van Dau F, Petroff F, Etienne P, Creuzet G, Friedrich A and Chazelas J 1988 *Phys. Rev. Lett.* **61** 2472
[2] Binash G, Grunberg P, Saurenbach F and Zinn W 1989 *Phys. Rev.* B **39** 4828
[3] Coey J M D, Berkowitz A E, Balcells L, Putris F F and Parker F T 1998 *Appl. Phys. Lett.* **72** 734
[4] Dowben P A and Skomski R 2003 *J. Appl. Phys.* **93** 7948
[5] Eerenstein W, Palstra T T M, Hibma T and Celotto S 2003 *Phys. Rev.* B **68** 014428
[6] Eerenstein W, Palstra T T M, Hibma T and Celotto S 2002 *Phys. Rev.* B **88** 247204
[7] Seneor P, Fert A, Montaigne F, Petroff F and Vaurs A 1999 *Appl. Phys. Lett.* **74** 4017
[8] Ziese M and Blythe H J 2000 *J. Phys.: Condens. Matter* **12** 13
[9] Margulies D T, Parker F T, Rudee M L, Spada F E, Chapman J N, Aitchison P R and Berkowitz A E 1997 *Phys. Rev.* B **79** 5162
[10] Terrier C, Abid M, Arm C, Serrano-Guisan S, Gravier L and Ansermet J-Ph 2005 *J. Appl. Phys.* **98** 086102
[11] Gravier L, Fàbian A, Rudolf A, Cahin A, Wegrove J E and Ansermet J-Ph 2004 *Meas. Sci. Technol.* **15** 420
[12] Bauminger R, Cohen S G, Marinov A, Ofer S and Segal E 1961 *Phys. Rev.* **122** 1447
[13] Fujii T, Takano M, Katano R, Bando Y and Isozumi Y 1989 *J. Appl. Phys.* **66** 3168
[14] Fujii T, Takano M, Katano R, Bando Y and Isozumi Y 1990 *J. Cryst. Growth* **99** 606
[15] Daniels J M and Rosenswaig A 1969 *J. Phys. Chem. Solids* **30** 1561
[16] Constantin C and Rosenberg M 1971 *Solid. State Commun.* **9** 675
[17] Kuipers A J M and Brabers V A M 1976 *Phys. Rev.* B **14** 1401
[18] Lavine J M 1959 *Phys. Rev.* **114** 482
[19] Griffiths B A, Elwell D and Parker R 1970 *Phil. Mag.* **22** 163
[20] Gong G Q, Gupta A, Xiao G, Qian W and Dravid V P 1997 *Phys. Rev.* B **56** 5096
[21] Sheng P 1980 *Phys. Rev.* B **21** 2180
[22] Sondheimer E H 1952 *Adv. Phys.* **1** 1
[23] Liu H, Jiang E Y, Bai H L, Zheng R K and Zhang X X 2003 *J. Phys. D: Appl. Phys.* **36** 2950
[24] Verwey E J W 1939 *Nature* **144** 327
[25] Park C, Peng Y, Zhu J G, Laughlin D E and White R M 2005 *J. Appl. Phys.* **97** 10C303
[26] Kneller E F and Luberosky 1963 *J. Appl. Phys.* **34** 656
[27] O'Grady K and Chantrell R W 1992 *Magnetic Properties of Fine Particles* ed J L Dormann and D Fiorani (Amsterdam: North-Holland) p 93
[28] Del Bianco L A J M and Brabers V A M 2002 *Phys. Rev.* B **66** 174418
[29] Ziese M, Hohne R, Semmelhack H C, Reckentin H, Hong N H and Esquinazi P 2002 *Eur. Phys. J.* B **28** 415
[30] Evetts J E, Blamire M G, Mathur N D, Isaac S P, Teo B S, Cohen L F and Macmanus-Driscoll J L 1998 *Trans. R. Soc. Lond.* A **356** 1593
[31] Savini L 2002 *J. Appl. Phys.* **91** 8593